INTERNATIONAL JOURNAL FOR NUMERICAL METHODS IN FLUIDS, VOL. 12, 609–624 (1991)

EXAMINATION OF WALL DAMPING FOR THE k–ε TURBULENCE MODEL USING DIRECT SIMULATIONS OF TURBULENT CHANNEL FLOW

E. WADE MINER, THOMAS F. SWEAN JR., ROBERT A. HANDLER AND RICHARD I. LEIGHTON

Center for Fluid Dynamic Developments, Laboratory for Computational Physics and Fluid Dynamics, U.S. Naval Research Laboratory, Washington, DC 20375, U.S.A.

SUMMARY

Handler, Hendricks and Leighton have recently reported results for the direct numerical simulation (DNS) of a turbulent channel flow at moderate Reynolds number. These data are used to evaluate the terms in the exact and modelled transport equations for the turbulence kinetic energy k and the isotropic dissipation function ε. Both modelled transport equations show significant imbalances in the high-shear region near the channel walls. The model for the eddy viscosity is found to yield distributions for the production terms which do not agree well with the distributions calculated from the DNS data. The source of the imbalance is attributed to the wall-damping function required in eddy viscosity models for turbulent flows near walls. Several models for the damping function are examined, and it is found that the models do not vary across the channel as does the damping when evaluated from the DNS data. The Lam–Bremhorst model and the standard van Driest model are found to give reasonable agreement with the DNS data. Modification of the van Driest model to include an effective origin yields very good agreement between the modelled production and the production calculated from the DNS data, and the imbalance in the modelled transport equations is significantly reduced.

KEY WORDS Wall damping k–ε model Channel flow Turbulence modelling Direct simulations

1. INTRODUCTION

During the past three decades the fluid dynamics community has focused considerable attention on the development of techniques and capabilities for the calculation of turbulent flow fields. Increases in available computational capabilities have permitted researchers to develop and test increasingly sophisticated and complete models for the numerical simulation of turbulent flows. The state of the art has reached a point where direct numerical simulations of turbulent flows at low-to-moderate Reynolds numbers are feasible. Such work has been reported in several studies, including those by Kim *et al.*[1] and Handler *et al.*[2] In these simulations the unsteady Navier–Stokes equations are solved numerically. All essential scales of the turbulent flow are resolved and no subgrid modelling of the turbulence is employed. Such calculations, however, are feasible only for research purposes, and calculations of turbulent flows for engineering purposes utilize the time-averaged Navier–Stokes equations coupled with some level of turbulence modelling.

For many applications the model of choice is the two-equation k–ε model. This model for turbulence transport came into use in the early 1970s based largely on the work of Hanjalić and

0271–2091/91/070609–16$08.00

Received November 1989
Revised May 1990

Launder[3] and Launder *et al.*[4] and became a standard because of its relative simplicity and success in providing good predictions for a large range of turbulent flows. In spite of some significant shortcomings in the k–ε model, it still retains a position as the standard for comparison.

In the development of the k–ε model, attention has been focused on high-Reynolds-number flows such as thin shear layers, and the constants in the model have been chosen to give agreement with experimental data for these flows. Consequently, the predictive capabilities of the model are best for strongly turbulent flows. For flows near fixed surfaces, adjustments to the model are needed. In References 3 and 4, boundary layer flows were treated by matching the high-Reynolds-number flow with wall functions, e.g. 'law-of-the-wall' profiles, at the first grid point away from the wall. In that way the model did not have to be directly modified for the low-Reynolds-number flow adjacent to the wall. In work since then, Hanjalić and Launder[5] and a number of researchers have proposed extensions to the basic high-Reynolds-number model that would enable the k–ε model to be directly used all the way to the wall. Patel *et al.*[6] reviewed a number of near-wall models and found that while the better ones did quite well, there were still areas where improvement was needed. One of the limitations in the development of near-wall models has been the difficulty in making accurate and reliable measurements of the flow quantities near the wall so that some of the correlations that are needed in improving the k–ε model cannot be obtained experimentally.

Data from direct numerical simulations of turbulent flows can be used in place of experimental data in evaluating and improving the near-wall turbulence models. Mansour *et al.*[7] have used the data of Kim *et al.*[1] to analyse the terms in the modelled transport equations for the Reynolds stresses and for ε. They have also used those data to analyse the terms in the modelled transport equation for the turbulence kinetic energy.[8] They show that some of the models are inadequate but do not make specific recommendations for improvement. In this study we use the direct simulation data of Handler *et al.*[2] to examine the terms in the k–ε model, with particular emphasis on the behaviour of the terms near the wall. Since the wall damping for the eddy viscosity has a crucial role in the accuracy of any near-wall k–ε model, we use the direct simulation data to examine the three models which Patel *et al.*[6] found to perform well and two other models. In the next two sections we discuss briefly the direct simulation calculations and the exact and modelled k–ε transport equations. In Section 4 we evaluate the terms in the exact and modelled transport equations and compare the damping given by the near-wall models with the damping indicated by the direct simulation data. We then show that improved agreement between the exact and modelled results can be obtained.

2. DIRECT NUMERICAL SIMULATION

Numerical methods are being developed at the U.S. Naval Research Laboratory (NRL) for the direct numerical simulation (DNS) of turbulent flows. Much of the background for this effort is provided in the study by Handler *et al.*,[2] hereinafter referred to as HHL. In their report, HHL review several numerical methods for pseudo-spectral calculations and present the results of applying these methods to the computation of turbulent channel flows. Several calculations parametrized by the extent of the physical domain, grid resolution and Reynolds number are described. In this study we use the Chan 1.1 data of HHL. This is one of their lower-resolution (spatial) data sets; however, it is one for which complete velocity and pressure are available at widely spaced time intervals, thus insuring that the separate realizations are statistically independent.

In units of channel half-width h the channel dimensions are $2 \times 5 \times 5$ in the vertical (x_2), streamwise (x_1) and lateral (x_3) directions respectively. The flow is computed with 16×64 evenly

spaced grid points in the horizontal (x_1–x_3) plane and 33 points with Chebyshev scaling are used in the x_2-direction. The Reynolds number Re is 2215 based on h and U_0, the initial laminar centreline velocity. The governing equations are non-dimensionalized by the wall shear velocity, a viscous length unit and a viscous time unit. The wall shear velocity u_τ is given by

$$u_\tau = \left(\nu \left. \frac{\partial \overline{U_1}}{\partial x_2} \right|_w \right)^{1/2}.$$

The viscous length unit (or wall unit) is $l_v = \nu/u_\tau$ and the viscous time unit is $t_v = \nu/u_\tau^2$. In the non-dimensionalized units the Reynolds number based on the wall shear velocity is 125. This is lower than the wall Reynolds number of 180 for the Kim *et al.*[1] (hereinafter referred to as KMM) data and the grid resolution of the Chan 1.1 data is lower. HHL conclude, however, that the mean statistics of their data set compare well with experiment and with the more highly resolved data of KMM insofar as one-point statistics are concerned.

The equations are solved using a pseudo-spectral method in which Chebyshev expansion is used in the wall normal (x_2) direction and Fourier series are used in the streamwise (x_1) and spanwise (x_3) directions. The domain size in wall units is 640, 250 and 640 in the x_1-, x_2- and x_3-direction respectively. In the x_2-direction the use of Chebyshev polynomials gives a variable step size, with $\Delta x_2 \approx 0{\cdot}6$ at the wall and $\Delta x_2 \approx 12$ at the channel centre. In the x_1- and x_3-direction the step size is uniform and is $\Delta x_1 \approx 40$ and $\Delta x_3 \approx 10$ respectively. In the computed data set used in the present work there are 33 distinct realizations of the velocity and pressure fields which are separated by 50 viscous time units. This separation in time is sufficient to insure that each realization of the fields is statistically independent.

We denote the instantaneous values of variables by uppercase symbols, the time-averaged values with an overbar and the fluctuations from the time averages by lowercase symbols so that, for example,

$$U_i(t) = \overline{U_i} + u_i(t), \qquad P(t) = \bar{P} + p(t).$$

Also, we denote the turbulence intensities as $u_i' = \sqrt{\overline{u_i^2}}$. The velocity field in the channel is periodic in the x_1- and x_3-direction so that averaging over the x_1–x_3 plane at each value of x_2 gives dependent variable profiles which are functions of the wall normal co-ordinate (x_2). Averages are obtained by summing the individual profiles over 33 separate realizations. Correlations of the fluctuating variables such as $\overline{u_1 u_2}$ are computed by forming the product at each grid point in the domain, averaging over the x_1–x_3 plane and then averaging over the 33 realizations.

The primary averaged data from the direct numerical simulation of channel flow by HHL are shown in Figures 1 and 2. Figure 1 shows the mean streamwise velocity $\overline{U_1}$ and the root mean square (RMS) of the pressure fluctuations p'. The velocity profile shows a fully developed turbulent flow profile with a channel centre value of 17. The RMS of the pressure fluctuations shows peaks of 1·9 at $y/h = \pm 100$. At the channel centre, p' has a minimum value less than 1·0. The values at the walls are between 1·2 and 1·3. These data are described in HHL and are noted to be in overall good agreement with KMM considering the differences in Reynolds number. Figure 2 shows the turbulence intensities u_1', u_2', u_3' and the Reynolds shear stress $\overline{u_1 u_2}$. The Reynolds shear stress shows peak values of $\pm 0{\cdot}65$ at $y/h = \pm 95$ and linear variation over the interval $-85 < y/h < 85$. The averaged data in these figures exhibit excellent overall symmetry between the channel walls. It is noted by HHL that the locations of the peak values of u_i' are in excellent agreement with the data of KMM and experimental data, although the maxima are slightly lower. The variances are attributable to the different Reynolds numbers in the simulations and, to a lesser extent, to the finer resolution of the KMM data.

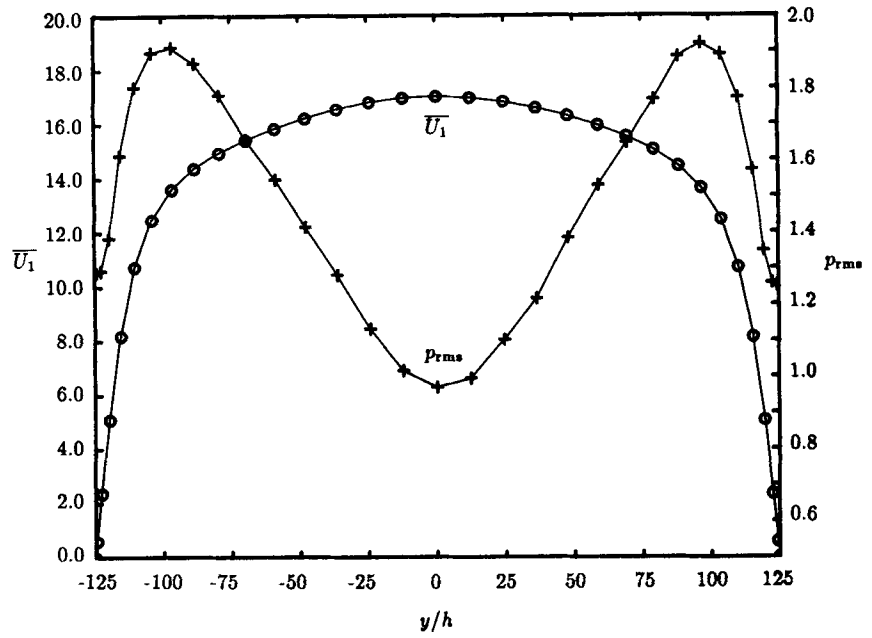

Figure 1. Profiles of mean streamwise velocity $\overline{U_1}$ and root mean square of pressure fluctuations p' from the direct simulation data of Handler *et al.*[1]

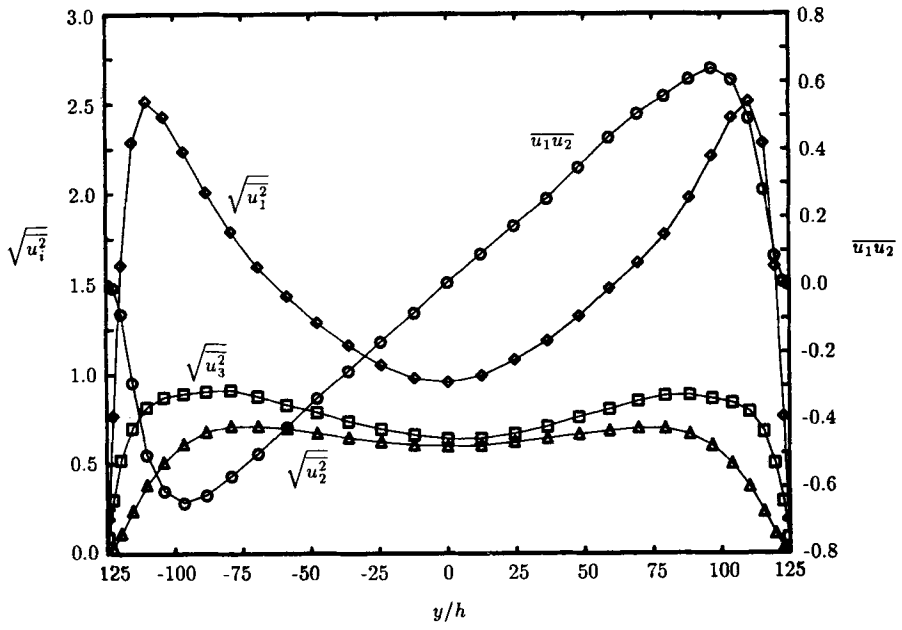

Figure 2. Profiles of turbulence intensities $\sqrt{\overline{u_i^2}}$ and Reynolds shear stress $\overline{u_1u_2}$ from the HHL data

3. THE k–ε TRANSPORT EQUATIONS

Exact transport equations

The two-equation k–ε model for turbulent flow requires transport equations for the turbulence kinetic energy k and for ε, the rate of dissipation of turbulence energy. The exact equation for the transport of turbulence kinetic energy is obtained from the sum of the transport equations for the three normal Reynolds stresses, and for incompressible fluids is given by Hinze[9] as

$$\underset{\text{(i)}}{\frac{Dk}{Dt}} = \underset{\text{(i)}}{-\overline{u_i u_j}\frac{\partial \overline{U_j}}{\partial x_i}} \underset{\text{(ii)}}{-\frac{\partial}{\partial x_i}(\overline{u_i k'})} \underset{\text{(iii)}}{-\frac{\partial}{\partial x_i}\left(\overline{u_i \frac{p}{\rho}}\right)} \underset{\text{(iv)}}{+\nu\frac{\partial^2}{\partial x_i \partial x_i}k} \underset{\text{(v)}}{-\nu\overline{\frac{\partial u_j}{\partial x_i}\frac{\partial u_j}{\partial x_i}}}, \tag{1}$$

where k' is half the sum of the normal stresses and k is its averaged value, and D/Dt is the substantial derivative.

The terms on the right-hand side correspond to rate of (i) production of turbulence kinetic energy, (ii) kinetic energy diffusion, (iii) pressure diffusion, (iv) viscous diffusion and (v) viscous dissipation of turbulence kinetic energy. Term (v) is strictly the viscous dissipation only for homogeneous turbulence. However, as pointed out by a reviewer, it may be shown to apply also in high-Reynolds-number inhomogeneous turbulence since in that case

$$\varepsilon = \nu\overline{\frac{\partial u_i}{\partial x_j}\frac{\partial u_i}{\partial x_j}} + \nu\frac{\partial^2 \overline{u_i u_j}}{\partial x_i \partial x_j}$$

and the last term is negligible in high-Reynolds-number flows.

The exact transport equation for the dissipation rate ε is derived from the unsteady Navier–Stokes equations. We use the form given by Hanjalić and Launder,[5]

$$\begin{aligned}\underset{\text{(i)}}{\frac{D\varepsilon}{Dt}} = &\underset{\text{(i)}}{-2\nu\overline{\frac{\partial u_i}{\partial x_k}\frac{\partial u_i}{\partial x_l}\frac{\partial u_k}{\partial x_l}}} \underset{\text{(ii)}}{-2\overline{\left(\nu\frac{\partial^2 u_i}{\partial x_k \partial x_l}\right)^2}} \underset{\text{(iii)}}{-\frac{\partial}{\partial x_k}\left(\overline{u_k \varepsilon'} + \frac{2\nu}{\rho}\overline{\frac{\partial u_k}{\partial x_l}\frac{\partial p}{\partial x_l}}\right)} \underset{\text{(iv)}}{-\nu\frac{\partial \varepsilon}{\partial x_k}}\Bigg) \\ &\underset{\text{(vi)}}{-2\nu\left(\overline{\frac{\partial u_i}{\partial x_l}\frac{\partial u_k}{\partial x_l}} + \overline{\frac{\partial u_l}{\partial x_i}\frac{\partial u_l}{\partial x_k}}\right)\frac{\partial \overline{U_i}}{\partial x_k}} \underset{\text{(vii)}}{-2\nu\overline{u_k \frac{\partial u_i}{\partial x_l}}\frac{\partial^2 \overline{U_i}}{\partial x_k \partial x_l}}\end{aligned}, \tag{2}$$

where

$$\varepsilon = \nu\overline{\frac{\partial u_j}{\partial x_i}\frac{\partial u_j}{\partial x_i}}, \qquad \varepsilon' = \nu\frac{\partial u_j}{\partial x_i}\frac{\partial u_j}{\partial x_i}.$$

The first term (i) on the right-hand side of (2) represents turbulent production of ε and term (ii) represents dissipation of ε. Terms (iii), (iv) and (v) represent turbulent transport, pressure transport and viscous diffusion respectively. Terms (vi), (vii) and (viii) are production terms.

The individual terms in (1) and (2) have been calculated from the DNS data of HHL. For the channel flow simulations the mean flow is homogeneous in the horizontal co-ordinate directions so that $\overline{U_1} = f(x_2)$ and $\overline{U_2} = \overline{U_3} = 0$. Because of symmetry with respect to planes normal to the spanwise direction, all correlations involving u_3 and uneven derivatives with respect to x_3 are zero. Products such as $u_i u_j$ are formed at each grid point in the domain; the correlation is then

averaged over the x_1–x_3 plane to give a profile in x_2. The x_2-profiles are then averaged over the 33 realizations in the saved data set. In forming the averages of the terms we make use of the symmetry (in the mean) of the channel flow about the centreline. In the following figures we use the wall normal distance $y^+ = yu_\tau/\nu$ with origin at the wall, whereas in the preceding figures we used y/h with origin at the channel centre.

The individual terms in (1) are shown in Figure 3. In this and the following figures a gain denotes a term contributing to a local increase in the transported quantity and a loss denotes a term contributing to a local decrease. The two dominant terms are the production and dissipation. The dissipation is small at the channel centre and increases towards the wall, with its maximum at the wall. The production is zero at the channel centre and at the wall and has a maximum at $y^+ = 20$. The kinetic energy diffusion (or turbulent transport) balances the dissipation at the channel centre, goes to zero at about $y^+ = 35$, has a minimum at $y^+ = 20$, is positive for $y^+ < 10$ and is zero at the wall. The viscous diffusion (or gradient diffusion) is very small for $y^+ > 25$, has a minimum at $y^+ = 15$ and has a maximum at the wall where it balances the dissipation. The pressure diffusion (or pressure–velocity correlation) is very small across the channel.

As seen in Figure 4, across most of the channel the principal contribution to the transport of ε comes from terms (i) and (ii). Near the wall (for $y^+ < 25$) terms (vi) and (vii) become significant contributors and very near the wall (for $y^+ < 3$) term (v) becomes a major contributor. At the wall it is term (v) which balances term (ii). The other three terms ((iii), (iv) and (viii)) contribute very little to the transport of ε in the channel and are not shown in this figure.

For engineering calculations of turbulent flows the k–ε model is adequate for many applications, but (1) and (2) cannot be used directly. The terms involving the fluctuating velocity and pressure components must be modelled. The models which are in use have been developed on the basis of order-of-magnitude analysis of the transport equations and contain empirical constants which have been determined from experimental data. The experimental database is incomplete because of difficulties of measuring some of the terms in the exact equations. The data from the

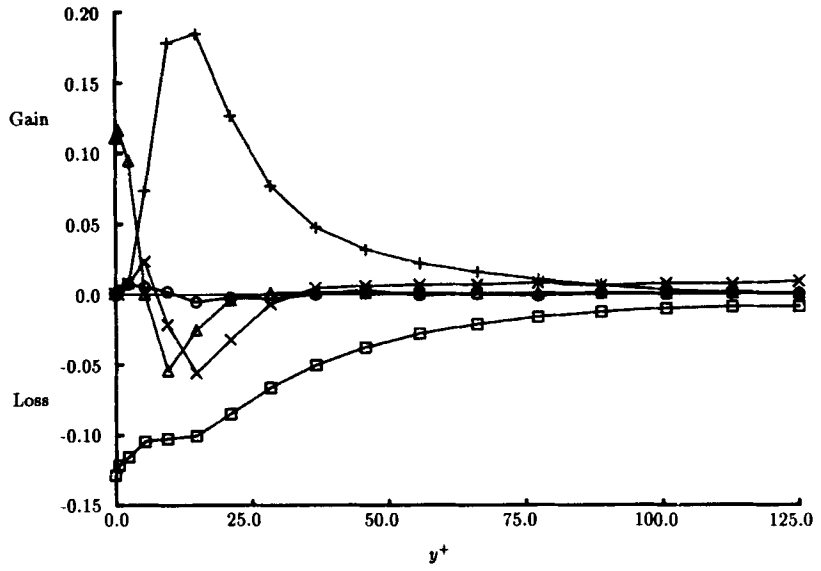

Figure 3. Budgets of the terms of the exact k-transport equation for incompressible flow: production term $\mathscr{P}$ (+); kinetic energy diffusion (×); pressure diffusion (○); viscous diffusion of k (△); homogeneous viscous dissipation ε (□)

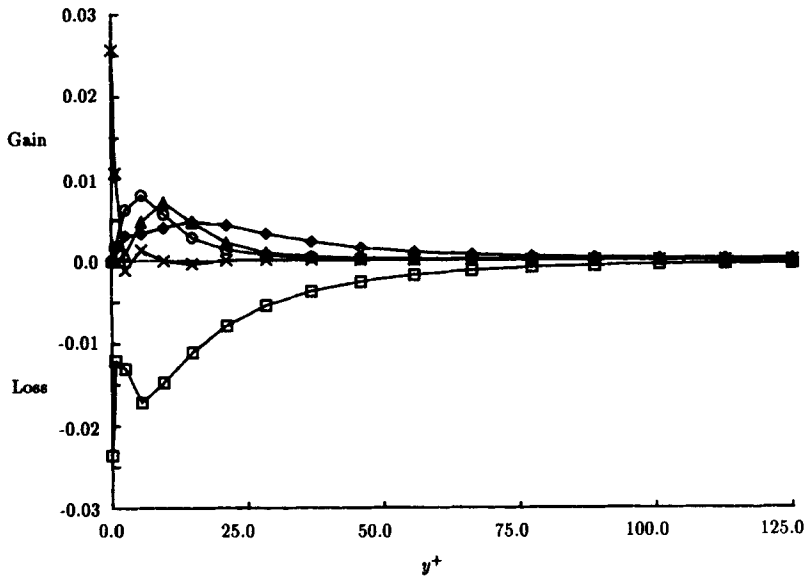

Figure 4. Budgets of the principal terms of the exact ε-transport equation: turbulent production of ε ($\diamond$); dissipation of ε ($\square$); viscous diffusion ($\times$); production terms (vi) ($\circ$) and (vii) ($\triangle$)

direct simulations permit a precise examination of the terms in the transport equations and a direct evaluation of the turbulence models.

Modelled transport equations

The derivation of the modelled transport equations is given by Rodi[10] and others. Central to the development of the models is the representation of the Reynolds stresses using the Boussinesq eddy viscosity relation. For fully developed channel flow, $\overline{U_2}$ and $\overline{U_3}$ are zero, as are the derivatives of the averaged turbulence variables in the x_1- and x_3-direction. Also, the time derivatives of k and ε are zero and the modelled transport equations reduce to the form

$$\frac{Dk}{Dt}=0=\frac{\partial}{\partial x_2}\left[\left(\nu+\frac{\nu_t}{\sigma_k}\right)\frac{\partial k}{\partial x_2}\right]+\mathscr{P}-\varepsilon, \tag{3}$$

$$\frac{D\varepsilon}{Dt}=0=\frac{\partial}{\partial x_2}\left[\left(\nu+\frac{\nu_t}{\sigma_\varepsilon}\right)\frac{\partial \varepsilon}{\partial x_2}\right]+C_{\varepsilon 1}\frac{\varepsilon}{k}\mathscr{P}-C_{\varepsilon 2}\frac{\varepsilon^2}{k}, \tag{4}$$

where

$$\mathscr{P}=-\overline{u_1u_2}\frac{\partial \overline{U_1}}{\partial x_2}, \qquad -\overline{u_1u_2}=\nu_t\frac{\partial \overline{U_1}}{\partial x_2}, \qquad \nu_t=C_\mu f_\mu\frac{k^2}{\varepsilon}. \tag{5a, b, c}$$

Commonly accepted values of the constants σ_k, σ_ε, $C_{\varepsilon 1}$ and $C_{\varepsilon 2}$ are 1·0, 1·3, 1·44 and 1·92 respectively. In (5), C_μ is a constant and f_μ is a function to be determined by comparison with experimental data. For flows such as thin shear layers, $f_\mu=1{\cdot}0$ and the commonly accepted value for C_μ is 0·09, based on experimental flows for which the production $\mathscr{P}$ and dissipation ε are in approximate balance. However, as noted by Rodi,[10] for flows in which $\mathscr{P}$ and ε are unequal the

predictive ability of the k–ε model is improved by using C_μ as a function of $\mathscr{P}/\varepsilon$ such as the one which he determined from correlating experimental data. For wall-bounded flows, f_μ is the wall-damping function and is chosen to approach 1·0 when the flow is not influenced by the wall so as to be consistent with the thin shear layer model. Also, for wall-bounded flows the last term in (4) tends to infinity as the wall is approached since ε is non-zero and k^+ goes to zero at the wall. Hanjalić and Launder[5] alleviate this problem by replacing ε^2 by $\varepsilon\tilde{\varepsilon}$, where

$$\tilde{\varepsilon}=\varepsilon-2\nu\left(\frac{\partial k^{1/2}}{\partial x_2}\right)^2,$$

and the term $\varepsilon\tilde{\varepsilon}/k$ is bounded as x_2 goes to zero. Other researchers (see e.g. the review by Patel *et al.*[6]) use a different expression for $\tilde{\varepsilon}$ and/or a near-wall-damping function which drives the overall term to zero at the wall. Additionally, Launder and Sharma[11] and others use a transport equation for $\tilde{\varepsilon}$ instead of ε (as described in Reference 6).

4. EVALUATION OF THE k–ε MODEL

One of the significant differences between the k–ε turbulence model and models which require additional transport equations is in the treatment of the Reynolds stress terms $\overline{u_i u_j}$. In the models using separate equations for the transport of the Reynolds stresses, the $\overline{u_i u_j}$ terms are solved as unknown variables and higher-order terms are modelled. In the k–ε model the Reynolds stress terms are modelled using the eddy viscosity as given in (5c). The accuracy of this model is then central in considering the accuracy of the k–ε model.

If f_μ is taken to be 1·0, the k–ε model corresponds to the standard high-Reynolds-number model. Using the HHL data we have calculated the exact Reynolds shear stress and the shear stress as modelled by (5) with $C_\mu=0{\cdot}09$ and $f_\mu=1{\cdot}0$. The comparison of those data shows that the modelled shear agrees well with the exact shear in the centre of the channel but that in the near-wall region the modelled term is much larger than the Reynolds shear stress computed from the DNS data. The comparison shows that a damping term is required to bring the modelled Reynolds stress into better agreement with that calculated from the simulation data.

A number of researchers have focused attention upon application of the k–ε turbulence model in near-wall flows. Patel *et al.*[6] reviewed eight near-wall models of which seven were k–ε models. They found that three of the k–ε models performed reasonably well but that even those three models were in need of refinement. One of their principal conclusions was that an improved damping function for the eddy viscosity should be selected which was in agreement with experimental data and whose influence was restricted to the sublayer and the buffer zone.

In the modelled k-transport equation the terms for production, kinetic energy diffusion and pressure diffusion are modelled by expressions which involve ν_t and thus f_μ. By calculating the individual terms on the right-hand side of (3) using the direct simulation data of HHL, we find that the production term is the term most affected by changes in the wall-damping function. Similarly, for the modelled ε-transport equation the production term is the term which is most affected by changes in ν_t.

In the following we consider the wall damping of the three k–ε models which Patel *et al.*[6] found to perform well. These are the models of Launder and Sharma,[11] Chien[12] and Lam and Bremhorst.[13] We also include the van Driest[14] wall-damping model in our consideration. In the Launder–Sharma model the wall-damping function is given by

$$f_\mu=\exp[-3{\cdot}4/(1+R_T/50)^2], \tag{6a}$$

where R_T is a Reynolds number of turbulence given by $R_T = k^2/v\varepsilon$. The wall-damping function is

$$f_\mu = 1 - \exp(-0{\cdot}0115y^+) \tag{6b}$$

for the Chien model and

$$f_\mu = [1 - \exp(-0{\cdot}0165R_y)]^2\,(1 + 20{\cdot}5/R_T) \tag{6c}$$

for the Lam–Bremhorst model, where R_y is also a Reynolds number of turbulence and is given by $R_y = k^{1/2}y/v$. With the van Driest model the wall-damping function is given by

$$f_\mu = [1 - \exp(-y^+/A^+)]^2, \tag{6d}$$

where A^+ is a constant of the turbulence and 26·0 is the generally accepted value. In the Launder–Sharma and Chien models we use the appropriate expression for $\tilde{\varepsilon}$ (see Reference 6) instead of ε in the formulae for v_t and R_T.

We show in Figure 5 a comparison of the exact production term as calculated using the DNS data and the modelled production term with $f_\mu = 1{\cdot}0$. Noting the change in scale between Figure 5 and Figure 3, it is clearly seen that the modelled production is much too large in the neighbourhood of $y^+ = 15$. Also shown in Figure 5 is the modelled production term using the wall-damping function from the Launder–Sharma model and the Chien model. In order to obtain agreement with the DNS data, much more damping is required for $y^+ < 40$ than is provided by the Launder–Sharma model, and the Chien model requires more damping for $y^+ < 20$. For both models, agreement with the exact production term would be improved if ε were used in the expression for v_t instead of $\tilde{\varepsilon}$, and with the Chien damping the modelled term would be in close agreement with the exact term.

In Figure 6 we compare the exact production term with the modelled term using the Lam–Bremhorst and van Driest wall-damping models. In Figure 6 the axis scales are the same as in Figure 3 and it is seen that the Lam–Bremhorst model gives better agreement with the DNS

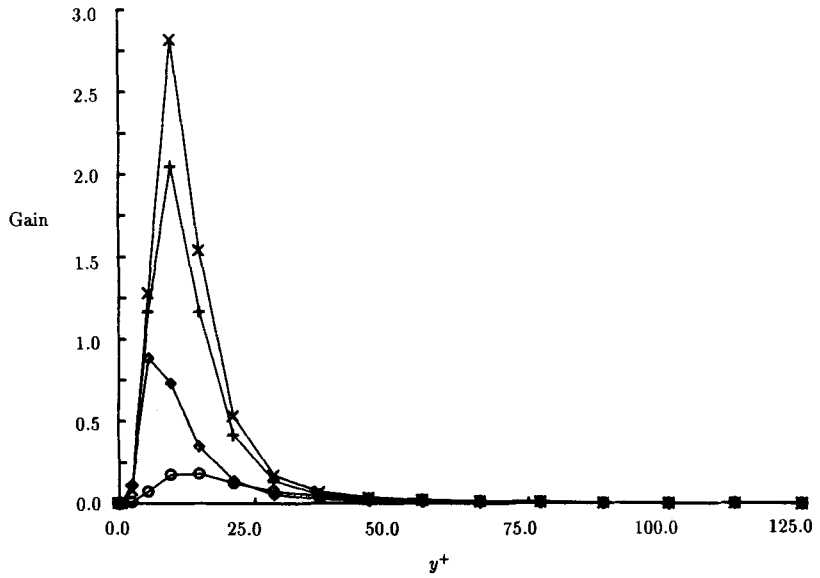

Figure 5. Comparison of the exact k-transport equation production term (○) with the undamped modelled term (×), the modelled term damped with the Launder–Sharma damping (+) and the Chien wall damping (◇)

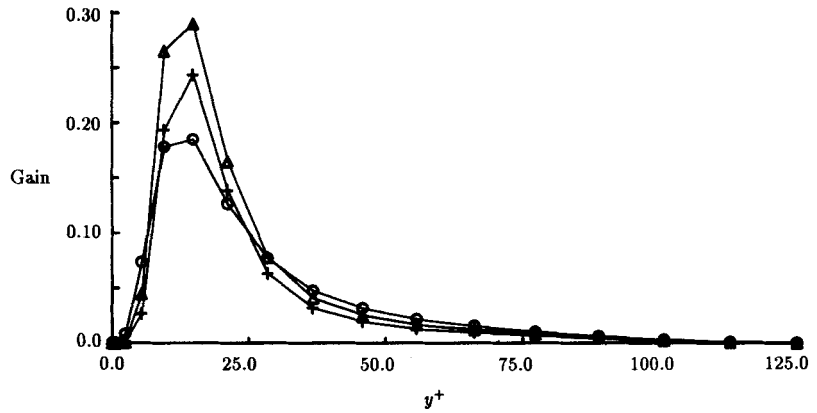

Figure 6. Comparison of the exact k-transport equation production term (○) with the modelled term using the Lam–Bremhorst wall damping (+) and the standard van Driest wall damping (△)

data for $y^+ < 25$. At $y^+ \approx 20$ the van Driest model yields a higher value for $\mathscr{P}$ than is given by the DNS data or the Lam–Bremhorst model. For $y^+ > 25$ the Lam–Bremhorst model gives values of $\mathscr{P}$ less than the values from the van Driest model and the DNS data.

Since the principal variable in modelling the production term is the wall-damping function, the modelled production can be brought into better agreement with $\mathscr{P}$ calculated from the DNS data with an improved wall-damping function. Figure 7 shows the damping functions from the Chien, Lam–Bremhorst, Launder–Sharma and van Driest models. The figure also includes the distribution of f_μ when it calculated from the DNS data using

$$f_\mu = -\overline{u_1 u_2}\,\frac{\varepsilon}{C_\mu k^2}\left(\frac{\partial \overline{U_1}}{\partial x_2}\right)^{-1}. \tag{7}$$

In evaluating (7), C_μ is chosen so that the calculated f_μ goes to 1·0 at the channel centre. For this channel flow, $C_\mu = 0{\cdot}115$ gives $f_\mu = 1{\cdot}0$ at the channel centre. Since at the wall $k = 0$ and at the channel centre $\partial \overline{U_1}/\partial x_2 = 0$, evaluation of (7) is limited to the interval $0 < y^+ < 125$.

Also included in Figure 7 as the filled rectangles are some of the data for f_μ which Patel *et al.* derived from experimental data and presented in their Figure 2. The experimental data were calculated[15] from the data for k^+, $\overline{uv}^+$ and ε^+ using the mean curves shown in Figure 1 of Reference 6 and $\mathrm{d}\overline{U}^+/\mathrm{d}y^+$ from equation (12) of Reference 6. It is difficult to assess the accuracy of the values of f_μ derived from the experimental data, especially since some of the terms in ε cannot be measured near a wall. Patel *et al.* show the mean curve for ε following the pipe data of Laufer[16] and he determined that the dissipation summed across the cross-section agreed with the total production of k^+ to within 10%.

As calculated from the DNS data using (7), f_μ has a minimum value of 0·04 at $y^+ = 6$ and then increases towards the wall. Such a characteristic also appears in the experimental data of Patel *et al.* for f_μ. The experimental data for f_μ are in good agreement with the HHL data and show a non-zero minimum at about $y^+ = 7$. Expansion of the terms of (7) in Taylor series about $y^+ = 0$ shows that for small y^+, $u_1 = ay^+ + \ldots$, $u_2 \to by^{+2} + \ldots$, $u_1 u_2 \to cy^{+3} + \ldots$, $\varepsilon' \to d + ey^+ + \ldots$ and $k' \to gy^{+2} + \ldots$. Since near the wall $\partial \overline{U_1}/\partial x_2$ is constant, the damping function in (7) must vary as $h/y^+ + j + \ldots$. The result of this simple analysis is difficult to work with since it contains a singularity, but it does indicate that f_μ should have a minimum

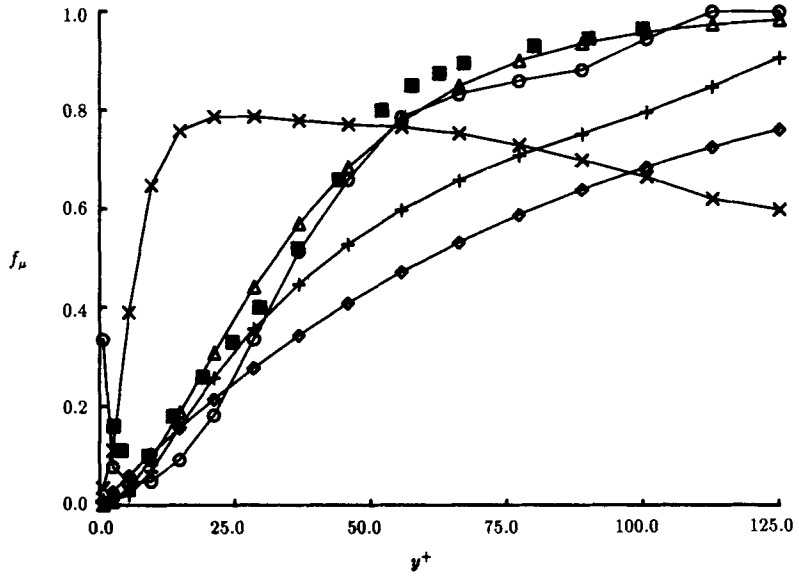

Figure 7. Comparison of the wall-damping function f_μ from the experimental data of Patel *et al.* (■), calculated from the HHL data, equation (7) (○), from the Chien model (◇), the Lam–Bremhorst model (+), the Launder–Sharma model (×) and the standard van Driest model (△). For HHL data, $C_\mu = 0{\cdot}115$ to give $f_\mu = 1{\cdot}0$ at channel centre.

located off the wall. None of the wall-damping models vary as $1/y^+$ for small y^+ and most go to zero instead of to a non-zero minimum.

As shown in Figure 7, the Launder–Sharma model damping is the least like the DNS or the experimental data, while across most of the channel the van Driest model is closest to the DNS data. However, in the neighbourhood of $y^+ = 10$, where the production is greatest, the Lam–Bremhorst damping model agrees best with the DNS data and thus the Lam–Bremhorst model gives the best overall agreement for the maximum value of the production term, as seen earlier.

Of the four damping models shown in Figure 7, f_μ for the van Driest model is the most similar to f_μ from the HHL data. Introducing an effective origin y_0^+ in (7) improves the agreement with f_μ from the HHL data. Agreement is further improved by modifying the equation so that f_μ has a minimum value f_0 corresponding to the minimum from the HHL data. With these modifications the damping function is given by

$$f_\mu = f_0 + (1 - f_0)\{1 - \exp[-(y^+ - y_0^+)/A^+]\}^2. \tag{8}$$

Figure 8 shows a comparison between f_μ from the HHL data and f_μ from (8) with $y_0^+ = 8$ and $f_0 = 0{\cdot}04$. The agreement is seen to be very good. Also shown in this figure are the experimental data from Patel *et al.* which were included in Figure 7. The modifications to the van Driest wall-damping function seem to be consistent with the experimental data and give very good agreement with the direct simulation data. With f_μ given by (8) and with $C_\mu = 0{\cdot}115$ the modelled production term agrees very well with the exact production term from the HHL data as is shown in Figure 9.

With the modified van Driest model for f_μ, most of the imbalance in the budget of the terms in the modelled k-transport equation is contributed by the model for the sum of the pressure diffusion and kinetic energy diffusion terms. Figure 10 shows the overall imbalance for the modelled k-transport equation and the difference in the modelled and exact diffusion terms. For

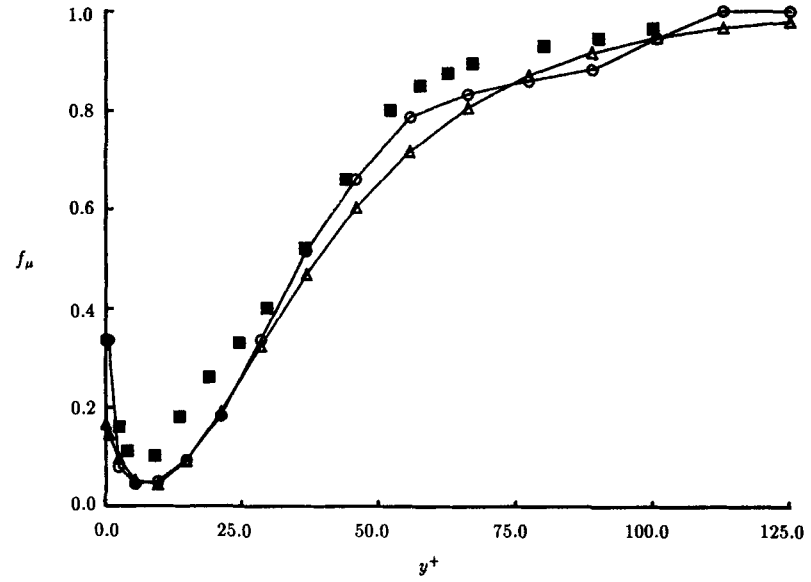

Figure 8. Comparison of the wall-damping function f_μ from the experimental data of Patel *et al.* (■), calculated from the HHL data, equation (7), with $C_\mu = 0{\cdot}115$ (○) and from the modified van Driest model, equation (18), with $y_0^+ = 8$ and $f_0 = 0{\cdot}04$ (△)

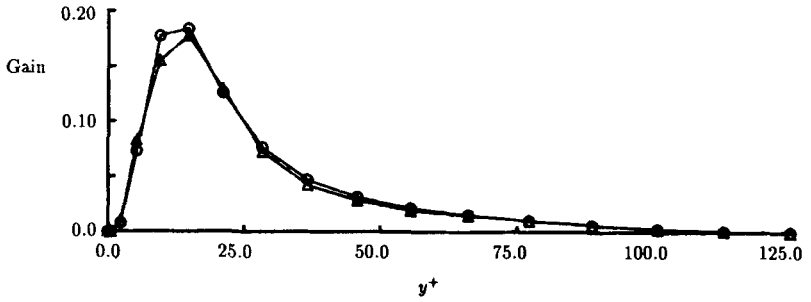

Figure 9. Comparison of the exact k-transport equation production term (○) with the production term modelled using the modified van Driest wall damping (△)

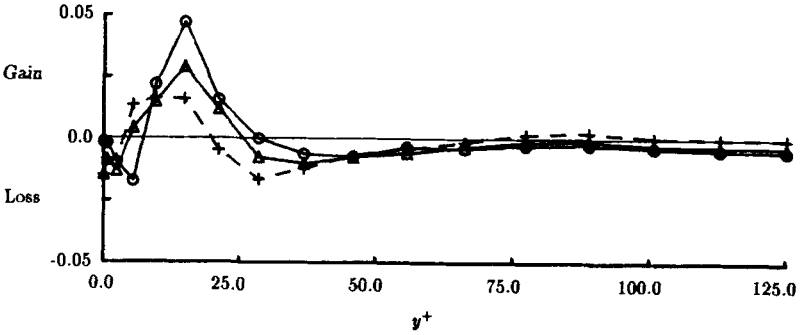

Figure 10. Comparison of the imbalance in the modelled k-transport equation (△ and +) with the difference between the model for the diffusion terms and the diffusion terms from the DNS data (○), for $\sigma_k = 1{\cdot}0$ (△) and $\sigma_k = 0{\cdot}6$ (+)

$y^+ < 25$ the difference in the modelled and exact diffusion terms is greater than the imbalance in the k-transport equation. It is possible to bring the model for the diffusion terms into slightly better agreement with the DNS data by adjusting the value of σ_k. For example, the dashed line in Figure 10 denotes the overall imbalance in the modelled turbulence kinetic energy transport equation when a value $\sigma_k = 0{\cdot}6$ is used in the evaluation of the diffusion term. Further reduction of the imbalance is not obtained with other values of σ_k. Better agreement is needed between the exact and modelled diffusion terms in order to decrease the imbalance further. The shape of the modelled term is not sufficiently similar to the shape of the terms from the exact transport equation, and a different functional is needed to improve the agreement between the modelled and exact diffusion terms.

The imbalance in the budget of the modelled ε-transport equation is also reduced with the modified van Driest wall damping. The diffusion term is quite small except very close to the wall and is essentially unaffected by the wall-damping models. The dissipation term is independent of the eddy viscosity and is here evaluated using $\varepsilon\tilde{\varepsilon}/k$. The production term is a major term and is directly proportional to the eddy viscosity. Figure 11 shows the distribution of the production terms and the overall imbalance using the Lam–Bremhorst and modified van Driest wall-damping models. The amount of imbalance is reduced by about one-half with the modified van Driest wall-damping model.

We have also investigated how further reductions in the imbalance of the modelled ε-transport equation might be obtained. For example, as noted by Mansour *et al.*,[7] the shape of term (ii) would be difficult to model while the combination of term (ii) with term (v) might be easier to model. However, no terms in the modelled equation correspond to the combination of terms (ii) and (v) in the exact equation. The production term in the modelled equation should correspond to either a combination of terms (vi) and (vii) or terms (i), (vi) and (vii) in the exact equation, but it does not agree well with either combination in shape or magnitude. Changes in the empirical constants in the modelled ε-transport equation do little to reduce the imbalance further. Thus we find that further improvements in the modelling of the ε-transport equation will require different model representations than are currently used.

The DNS data also make it possible to evaluate the validity of one of the basic assumptions of developing the k–ε model: that the production and dissipation of turbulence kinetic energy are in approximate balance. This assumption is valid for many flows but does not hold well for the channel. For the channel the production term must be zero at the wall and at the channel centre

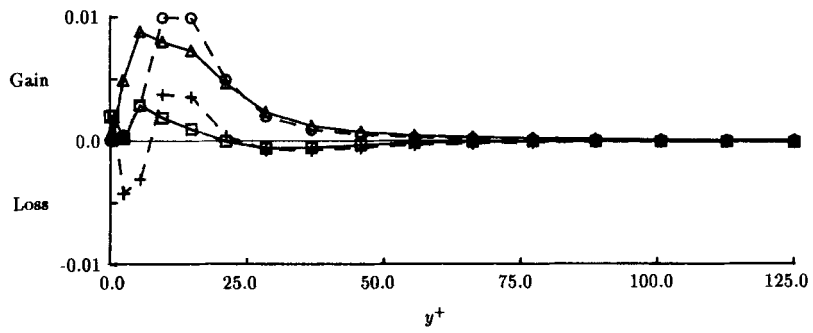

Figure 11. Comparison of the production terms (△ and ○) and the imbalance (□ and +) in the modelled ε-transport equation using the Lam–Bremhorst (○ and +, connected by dashed lines) and modified van Driest (△ and □, connected by solid lines) wall damping

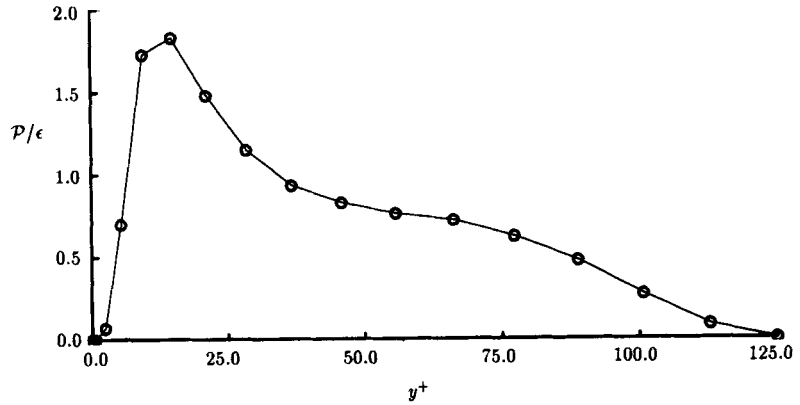

Figure 12. Distribution across the channel of the ratio of the production of turbulence kinetic energy, $\mathcal{P}$, to the dissipation rate ε as calculated from the direct simulation data

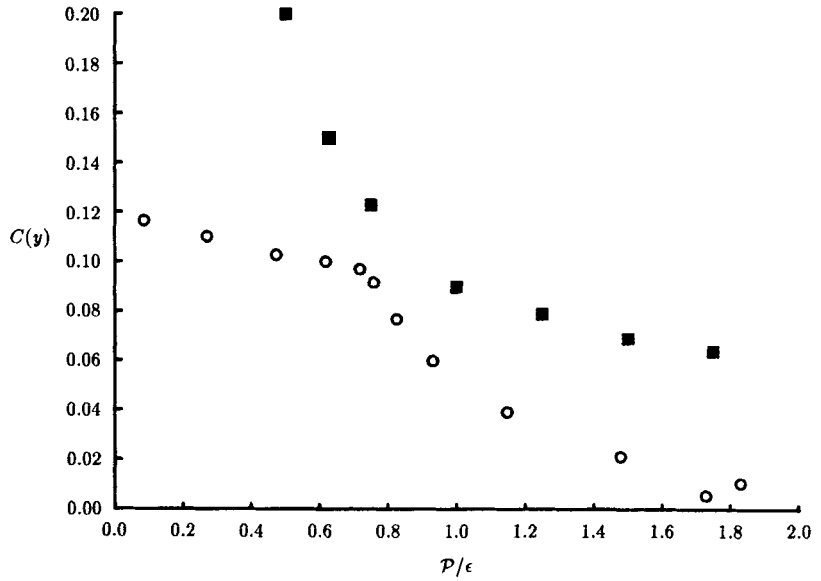

Figure 13. The eddy viscosity coefficient $C(y)$ as a function of the ratio of the production of turbulence kinetic energy, $\mathcal{P}$, to the dissipation rate ε from the HHL direct simulation data (○), together with data from Rodi's correlation of experimental data (■)

since $\overline{u_i u_j} = 0$ at the wall and $\partial \overline{U_1}/\partial x_2 = 0$ at the channel centre. The variation across the channel of the ratio $\mathcal{P}/\varepsilon$ from the DNS data is shown in Figure 12. The peak value of $\mathcal{P}/\varepsilon$ is approximately 1·9 and occurs in the near-wall region at $y^+ = 15$. For $10 < y^+ < 35$ the ratio is greater than 1·0, but averaged across the channel $\mathcal{P}/\varepsilon$ is 0·7. Thus for the channel a value for C_μ other than 0·09 is appropriate. Our use of $C_\mu = 0{\cdot}115$ with the modified van Driest damping function was based on using that value in (7) in order to obtain $f_\mu = 1{\cdot}0$ in the channel centre.

The larger value of C_μ is also suggested by the data which Rodi[10] gives from his correlation of experimental data for C_μ as a function of $\mathcal{P}/\varepsilon$. Representative values of that data are shown as the

filled symbols in Figure 13. Those data show that C_μ varies inversely with $\mathscr{P}/\varepsilon$. Denoting as $C_\mu(y)$ the product of C_μ and f_μ, we show in Figure 13 the values of $C_\mu(y)$ from the DNS data for the channel plotted versus $\mathscr{P}/\varepsilon$ in the region away from the wall. This also shows a distribution of $C_\mu(y)$ versus $\mathscr{P}/\varepsilon$ where $C_\mu(y)$ tends to vary inversely with $\mathscr{P}/\varepsilon$, except that $C_\mu(y)$ tends to level off to about 0·12 as $\mathscr{P}/\varepsilon$ decreases instead of continuing to increase as $\mathscr{P}/\varepsilon \to 0$ as is the case in Rodi's data.

5. CONCLUSIONS

In this study we have performed an evaluation of the k–ε turbulence model using the direct numerical simulation data of Handler *et al.* for turbulent channel flow. With the DNS data we have evaluated the terms of the exact k–ε transport equations and have found nearly exact agreement with the budget data presented by Mansour *et al.* Evaluation of the terms of the modelled transport equations shows the necessity of using a wall-damping function in the modelling of the eddy viscosity. From the HHL direct simulation data we have determined the shape required for a damping function to obtain agreement between the modelled turbulence kinetic energy production term and that calculated from the DNS data. We have shown that the well-accepted Lam–Bremhorst wall-damping model gives reasonable agreement with the DNS data.

We have also examined a number of currently used wall-damping models. The Lam–Bremhorst wall-damping model gives better agreement with the HHL direct simulation data than do the models of Chien and of Launder and Sharma. Compared with the van Driest damping model, the Lam–Bremhorst damping model gives better modelling of the production term near the wall where production is largest, but in the central part of the channel the van Driest damping models the production better. Except for a small region near the wall, the van Driest wall damping agrees best with the damping distribution calculated from the direct simulation data. Modification of the van Driest damping model to include an effective origin and a non-zero minimum gives very good agreement between the modelled production and the production calculated from the HHL data. With the modified van Driest damping function the principal contribution to the imbalance in the budget for the modelled turbulence kinetic energy transport equation comes from the model used for the sum of the pressure diffusion and kinetic energy diffusion terms.

We also find that the modified van Driest wall-damping function reduces the imbalance in the ε-transport equation when compared with the Lam–Bremhorst model. Further improvements in the modelling of the k- and ε-transport equations may be accomplished with the use of different functionals for the production and dissipation terms.

ACKNOWLEDGEMENTS

This work was supported by the Fluid Dynamics 6.1 Task Area of the Naval Research Laboratory. The channel code used in the current work was originally developed by Professor John McLaughlin (Clarkson University) and was modified by Steven Lyons (University of Illinois). The code was also modified at the Naval Research Laboratory to run efficiently on a Cray XMP 24. The authors also acknowledge the helpful comments of a reviewer.

REFERENCES

1. J. Kim, P. Moin and R. Moser, 'Turbulence statistics in fully developed channel flow at low Reynolds number', *J. Fluid Mech.*, **177**, 133–166 (1987).

2. R. A. Handler, E. W. Hendricks and R. I. Leighton, 'Low Reynolds number calculations of turbulent channel flow: a general discussion', *NRL Memorandum Report 6410*, Naval Research Laboratory, Washington, DC 1989.
3. K. Hanjalić and B. E. Launder, 'A Reynolds stress model of turbulence and its application to thin shear flows', *J. Fluid Mech.*, **52**, pt. 4, 609–638 (1972).
4. B. E. Launder, G. J. Reece and W. Rodi, 'Progress in the development of a Reynolds-stress turbulence closure', *J. Fluid Mech.*, **68**, pt. 3, 537–566 (1975).
5. K. Hanjalić and B. E. Launder, 'Contribution towards a Reynolds-stress closure for low-Reynolds-number turbulence', *J. Fluid Mech.*, **74**, pt. 4, 593–610 (1976).
6. V. C. Patel, W. Rodi and G. Scheuerer, 'Turbulence models for near-wall and low Reynolds number flows: a review', *AIAA J.*, **23**, 1308–1319 (1985).
7. N. N. Mansour, J. Kim and P. Moin, 'Reynolds-stress and dissipation-rate budgets in a turbulent channel flow', *J. Fluid Mech.*, **194**, 15–44 (1988).
8. N. N. Mansour, J. Kim and P. Moin, 'Near-wall k–ε turbulence modeling', *AIAA J.*, **27**, 1068–1073 (1989).
9. J. O. Hinze, *Turbulence*, McGraw-Hill, New York, 1975.
10. W. Rodi, *Turbulence Models and their Application in Hydraulics*, International Association for Hydraulic Research, Delft, 1980.
11. B. E. Launder and B. I. Sharma, 'Application of the energy–dissipation model of turbulence to the calculation of flow near a spinning disc', *Lett. Heat Mass Transfer*, **1**, 131–138 (1974).
12. K.-Y. Chien, 'Predictions of channel and boundary-layer flows with a low-Reynolds number turbulence model', *AIAA J.*, **20**, 33–38 (1982).
13. C. K. G. Lam and K. A. Bremhorst, 'Modified form of the k–ε-model for predicting wall turbulence', *J. Fluids Eng.*, **103**, 456–460 (1981).
14. E. R. van Driest, 'On turbulent flow near a wall', *J. Aeronaut. Sci.*, **23**, 1007–1011 (1956).
15. V. C. Patel, Private communication, 1990.
16. J. Laufer, 'The structure of turbulence in fully developed pipe flow', *NACA Report 1174*, 1954.